

This is an Open Access document downloaded from ORCA, Cardiff University's institutional repository: <https://orca.cardiff.ac.uk/id/eprint/134118/>

This is the author's version of a work that was submitted to / accepted for publication.

Citation for final published version:

Xu, Xiandong , Ming, Wenlong , Zhou, Yue and Wu, Jianzhong 2021. Unlocking the flexibility of combined heat and power for frequency response by coordinative control with batteries. *IEEE Transactions on Industrial Informatics* 17 (5) , pp. 3209-3219. 10.1109/TII.2020.3012495

Publishers page: <http://dx.doi.org/10.1109/TII.2020.3012495>

Please note:

Changes made as a result of publishing processes such as copy-editing, formatting and page numbers may not be reflected in this version. For the definitive version of this publication, please refer to the published source. You are advised to consult the publisher's version if you wish to cite this paper.

This version is being made available in accordance with publisher policies. See <http://orca.cf.ac.uk/policies.html> for usage policies. Copyright and moral rights for publications made available in ORCA are retained by the copyright holders.



Unlock the Flexibility of Combined Heat and Power for Frequency Response by Coordinative Control with Batteries

Xiandong Xu, Wenlong Ming, Yue Zhou, Jianzhong Wu

Abstract—Owners of combined heat and power (CHP), e.g., industrial manufacturers, are motivated to provide frequency response to power grids due to clear financial benefits. Yet, the slow response speed of CHP limits its capability in providing such services. Moreover, frequent adjustments would cause a faster lifetime reduction of CHP and rapid pressure fluctuation in the gas network. To further unlock the flexibility of CHP, this paper integrates a battery unit with CHP via a power electronic interface. A filter-based coordinative controller is designed for smoothing short-term fluctuations in CHP outputs. Based on the filter parameters and frequency response requirements, the minimum required capacity of the battery is identified. The results show that the proposed system enhances the capability of CHP for frequency response and mitigates the associated adverse effects on the gas network. The required capacity of the battery is economically feasible considering the benefit it brings to the CHP.

Index Terms—battery, CHP, coordinative control, flexibility, frequency response.

This work was supported in part by "UK Energy Research Centre Phase 4" (EP/S029575/1), EPSRC/NSFC CM2 (EP/T021969/1), EPSRC Supergen Energy Networks Hub (EP/S00078X/1), and FLEXIS (Flexible Integrated Energy Systems). FLEXIS is part-funded by the European Regional Development Fund (ERDF), through the Welsh Government. (*Corresponding authors: Yue Zhou and Jianzhong Wu*)

X. Xu, W. Ming, Y. Zhou, and J. Wu are with the School of Engineering, Cardiff University, Cardiff, CF24 3AA UK (e-mail: xux27@cardiff.ac.uk; mingw@cardiff.ac.uk; zhoy68@cardiff.ac.uk; wuj5@cardiff.ac.uk).

I. INTRODUCTION

In support of global decarbonization aspirations, intermittent renewable energy is given feed-in priority, which requires more flexible sources to support the power grid [1]. International Energy Agency's Status of Power System Transformation report highlights the need for actions to improve power system flexibility [2]. According to the Office of Gas and Electricity Markets (Ofgem) in Great Britain (GB), flexibility refers to 'modifying generation and/or consumption patterns in a reaction to an external signal (such as a change in price) to provide a service within the energy system' [3].

Thermal power plants have historically provided the flexibility. Due to carbon taxes and the retirement of aging power plants, fewer power plants are available. Meanwhile, decreasing inertia of power systems results in faster change of power system frequency and require more flexible resources [4]. Yet, building new plants requires not only a large amount of investment but also years to complete them [5]. Thus, utilities are looking at dispersed resources, such as energy storage and distributed generation, which have already been in operation.

Small-to-midsize combined heat and power (CHP) units, which are widely used in industries, are well positioned to provide flexibility services, pointed out by the U. S. Department of Energy [6]. A typical flexibility service, namely frequency response [7], [8], is one of the key areas where CHP has been attracting increased attention. A flexible CHP system at Princeton University which was designed to support campus' heat and electricity needs, has been applied to enable frequency response [9]. The CHP could extend beyond bill saving to flexibility services when other low emission sources are not available. Some studies have shown that CHP could enhance the frequency stability of the power grid in GB even only part of the total CHP capacity is employed [10]. Although providing flexibility may push the CHP deviating from the economic point, the payment from utilities is still attracting facility owners [11]. In a Belgium case, a decrease of 5% in the total energy cost was achieved via CHP regulation [12].

Yet, the flexibility of CHP for frequency response is partially locked by the physical limits of its equipment and the energy vectors to which it is connected [13], [14]. The available capacity of CHP that can be used

for frequency response is inherently limited due to its low ramp rate [15]. Moreover, different from conventional CHP applications that are scheduled hourly or quarter-hourly, frequency response requires CHP to achieve a quick change of generation in seconds. For example, the Firm Frequency Response (FFR) in GB requires participants to reach its maximum tendered capacity within 10s while a CHP can only adjust around half of its capacity in 60s [16]. A 6MW CHP generation with 0.1MW/s ramp rate could bid for a maximum of 1MW FFR in GB.

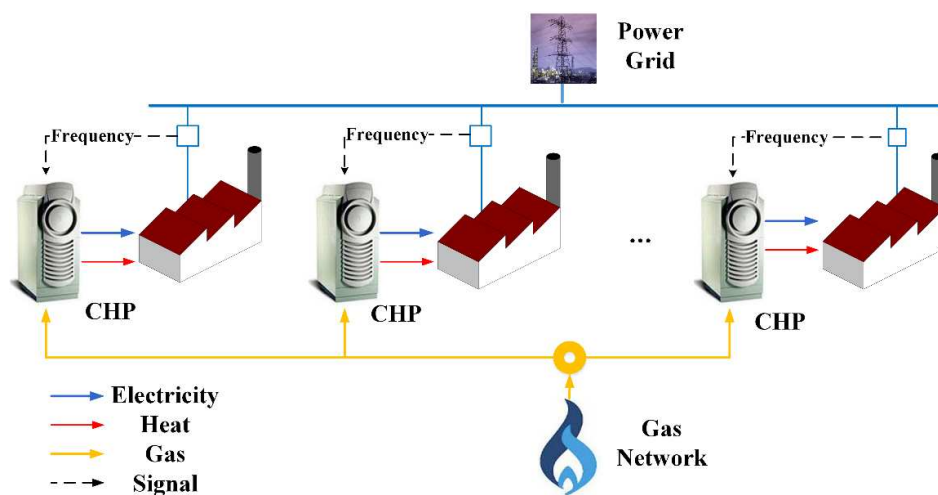


Fig. 1. Flexibility provision of CHPs to the power grid.

Moreover, providing dynamic frequency response would lead to frequent and uncertain adjustments in the CHP output. For example, the trigger frequency deviation for dynamic FFR in GB is ± 0.015 Hz away from the nominal frequency [17]. In Dec 2019, the amplitude of grid frequency deviations was above the trigger value 97.5% of the time [18]. Similar problems exist in dynamic frequency regulation in the US, such as Regulation D of PJM [19]. The adverse impact of these adjustments will drain away the profits of providing services to the power grid. This impact includes two aspects: 1) Frequent output adjustments reduce the lifetime of CHP. Unpredictable and overtime fluctuations would give rise to low cycle fatigue and creep failure of the turbines [20], [21]. The worst case as shown in Fig. 1 is that all CHPs taking part in the service change their generation at the same time when a frequency event occurs. 2) Fast frequency response may cause significant pressure fluctuation that goes beyond engineering or contract limits of the gas network. This

impact may be transferred back to the power grid and cause cascaded failure if not well managed [22]. Some studies have been conducted on mitigating this adverse impact [23]. Yet, the impact of fast CHP output change in seconds and the relevant solution are rarely analyzed.

A straightforward approach for increasing the ramp rate while avoiding frequent output regulation is to add energy storage into CHP. However, the power density and energy density should be carefully selected. Batteries, which are already installed in many sites for peak shaving [11] and improving energy efficiency [26], can also be used to support the frequency regulations. Li-ion battery's response time is less than 1s, which is fast enough for frequency response (e.g. 10s for primary response in GB) [27]. Some CHPs used in industries already have onboard batteries to support the startup and accelerating processes [28]. Considering the requirements of frequency response, how to choose a cheaper but effective battery is a big challenge. And it is also related to the behavior of CHP. Using CHP integrated with batteries to provide frequency response to the power grid has not been investigated.

To address this challenge, a coordinative control strategy for CHP and batteries is proposed to fully unlock the flexibility of CHP for frequency response. The capacity required for frequency response is used to generate the target for flexibility provision of CHP. A filter-based controller is designed to convert the target to set-points at slow and fast time scales for the CHP and battery. Based on the filter parameters and requirements of frequency response, the minimum power and energy capacities are identified for the battery. The salient features of this paper are summarized as follows:

- 1) According to CHP ramping restrictions, a guideline is given for designing the cut-off frequency of the filter-based controller, which was typically decided by trial and error.

- 2) A sizing scheme is proposed to help CHP owners identify the capacity of the battery for providing various amplitudes of frequency response. For a given CHP, the capacity of the battery is linearly proportional to the bidden capacity of frequency response. For different CHPs, the capacities of batteries are also affected by ramp rates.

- 3) The control scheme mitigates the impact of frequent regulations on the lifetime of CHP, as well as the

adverse impact of frequent CHP regulations on the gas network.

The rest of the paper is organized as follows. Section II provides a preliminary on the battery-assisted CHP (B-CHP) including system structure, operation modes, and its flexibility for frequency response. Section III proposes a coordinative controller for the battery and the generator of the CHP for providing frequency response services. Section IV presents a sizing scheme of batteries to support the coordinative control. Section V validates the proposed method using a real frequency event signal in GB, followed by a test in a simplified GB power system. The conclusions are drawn in Section VI.

II. PRELIMINARIES ON THE B-CHP

The B-CHP system embeds the CHP and the battery in one framework, which enhances the capability of the CHP in providing frequency response. Details are given as follows.

A. System Structure

Fig. 2 presents the B-CHP system. A single-shaft microturbine (MT), is employed as the CHP generator [28], [29]. The function of the onboard battery for supporting the start-up process and islanding operation is extended to provide frequency response to the power grid. As shown in Fig. 2, the B-CHP system consists of the MT-side system, the battery system, and the grid-side system. The MT takes fuel from the gas network and generates heat and high-frequency electricity. The electricity is converted to electricity at the grid frequency through a power electronic interface, i.e., the AC-DC and DC-AC converters. The battery system is connected to the DC link via a DC/DC converter. The voltage and current control loops in Fig. 2 are used to control the converters via Pulse Width Modulation (PWM) to follow the set-point of the power output at the grid-side u_{Grid} , the set-point of the power output of the battery u_{Bat} , and the set-point of the MT-side system u_{MT} .

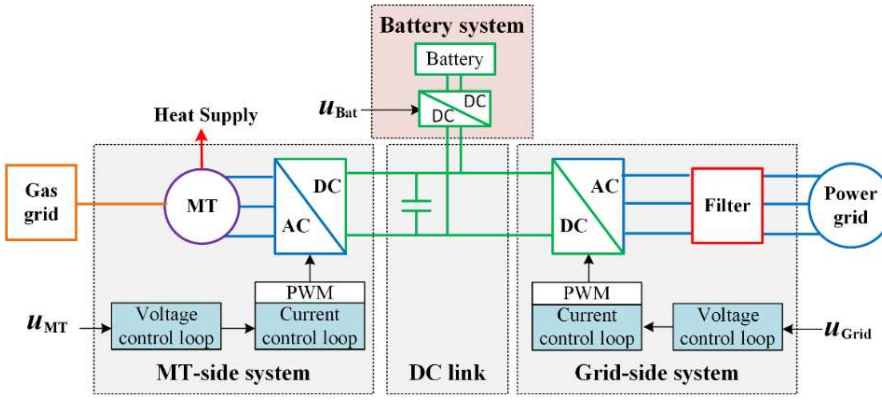


Fig. 2. Structure of the B-CHP system.

B. Operating Modes

Depending on whether a B-CHP is required to provide frequency response, two operating modes are considered within the control scheme, which leads to various target generation. The two operating modes are switched by modifying the controller of the MT-side system and the grid-side system.

The regular operation mode of the B-CHP is to follow either electricity or heat load signal. The CHP output is regulated by adjusting the fuel inlet position and further changing the turbine speed. Converter and inverter in Fig. 2 are controlled to follow the variations of MT output. The targeted CHP generation $P_{CHP,e}^{target}(t)$ is obtained based on the day-ahead schedule $P_{CHP,e}^{schedule}(t)$ and intra-hour adjustment $\Delta P_{CHP,e}^{DHS}(t)$ for addressing the imbalance in energy demand and supply.

$$P_{CHP,e}^{target}(t) = P_{CHP,e}^{schedule}(t) + \Delta P_{CHP,e}^{DHS}(t) \quad (1)$$

where $P_{CHP,e}^{min}$ and $P_{CHP,e}^{max}$ are the minimum and maximum electricity outputs of the CHP, $P_{CHP,e}^{min} \leq P_{CHP,e}^{target}(t) \leq P_{CHP,e}^{max}$.

In the frequency response mode, the electricity output of the B-CHP is adjusted to follow the frequency variation. For a given frequency deviation Δf , the relevant flexibility required by frequency response is defined as

$$P[\Delta f] = \begin{cases} k_{FR} \Delta f \frac{t}{T_r}, & 0 \leq t < T_r \\ k_{FR} \Delta f, & T_r \leq t \leq T_{FR} \end{cases} \quad (2)$$

where k_{FR} is the proportional gain for frequency response. Note that $P[\Delta f] \leq P_{bid}$, where P_{bid} is the bidding capacity of the B-CHP for frequency response. T_r is the required time for achieving full response capacity.

The flexibility demand is then added to the targeted CHP generation in the regulation mode as follow

$$P_{CHP,e}^{target}(t) = P_{CHP,e}^{schedule}(t) + \Delta P_{CHP,e}^{DHS}(t) + P[\Delta f] \quad (3)$$

Hereby it is assumed that thermal inertia of buildings accommodates CHP output's fluctuations smoothed by the battery. Long-term mismatches in heat supply and demand are handled by the intra-hour adjustment in the next period.

C. Flexibility Metrics for Frequency Response

This paper studies dynamic FFR balancing services in GB as an example to illustrate how a battery can unlock the flexibility of CHP in providing frequency response. Ramp rate, response amplitude, and duration are used as key metrics of the FFR [17].

Defining a flexibility function $F: R \mapsto R^3$, the flexibility demand of a frequency event $\Delta f(t)$ is described by

$$F[\Delta f(t)] = [R[\Delta f(t)] \quad P[\Delta f(t)] \quad E[\Delta f(t)]]^T \quad (4)$$

where $R[\Delta f(t)]$ is the ramp rate of flexibility provision, $R[\Delta f(t)] = \frac{dP[\Delta f(t)]}{dt}$. $P[\Delta f(t)]$ is the amplitude of flexibility provision. $E[\Delta f(t)]$ is the energy released by the frequency response asset during the flexibility provision period $[t_0, t_0 + T_{FR}]$, and $E[\Delta f(t)] = \int_{t_0}^{t_0 + T_{FR}} P[\Delta f(t)] dt$.

For a frequency response asset (CHP and battery in this paper), the flexibility is available with a period of T_{FR} if the following conditions are satisfied.

(C1) The derivative of the flexibility amplitude $P[\Delta f]$ along any frequency change $\Delta f(t) \in [\Delta f_{\underline{}}, \Delta f_{\overline{}}]$ is bounded within the limits for downward regulation \underline{R} and upward regulation \overline{R} , i.e.

$$R[\Delta f] \leq \left| \frac{P[\Delta \bar{f}] - P[\Delta \underline{f}]}{2T_r} \right| (1 + \varepsilon) \leq \min\{|\underline{R}|, \bar{R}\} \quad (5)$$

(C2) For a given flexibility provision period T_{FR} , the amplitude of flexibility satisfies

$$\underline{P}(t) \leq P[\Delta f(t)] \leq \bar{P}(t) \quad (6)$$

(C3) The available flexibility stored in the frequency response asset satisfies

$$\underline{E} - E_{base} \leq E[\Delta f(t)] \leq \bar{E} - E_{base} \quad (7)$$

where \bar{R} and \underline{R} are the maximum ramp up and ramp down rates of the frequency response asset. ε is the allowable tolerance for response error. $\Delta \bar{f}$ and $\Delta \underline{f}$ are the upper and lower bounds of frequency variations illustrated by the utility. $\bar{P}(t)$ and $\underline{P}(t)$ are the upper and lower bounds of the flexibility amplitude. \bar{E} and \underline{E} are the maximum and minimum stored energy in the frequency response asset. E_{base} is the stored energy in the asset.

III. COORDINATIVE SCHEME OF MT AND BATTERY FOR FREQUENCY RESPONSE

To deploy the flexibility of the B-CHP, this section proposes a two-level coordinative scheme for the battery and the MT, which includes an energy-sharing scheme at the upper level and a filter-based controller at the lower level.

A. Energy Sharing Between the Battery and MT

For a targeted power output signal u_{Grid} , the B-CHP changes its power output by controlling converters and the MT. Considering the different response speeds of converters and the MT, u_{Grid} is firstly converted to a slow ramp signal P_{MT}^{target} through a Butterworth filter. The signal is used to generate the speed reference and support the fuel control system to adjust MT output. The difference between u_{Grid} and P_{MT}^{target} is used to calculate u_{bat} for controlling the battery output.

At the power electronic interface, energy flows between the battery, MT and the power grid are adjusted by changing u_{Bat} and u_{Grid} . The MT converter is controlled to regulate DC link voltage at u_{MT} . Referring to

[30], a PQ control strategy is used at the grid-side converter, which ensures the rapid response of the B-CHP in following the variation of u_{Grid} .

The fuel supply to the MT is regulated by controlling speed, acceleration and exhaust temperature, as shown in Fig. 3. The reference speed is modified at various levels of power output through an optimal speed set-point generation block based on the torque-speed characteristics of MT. The speed reference is produced to ensure the MT to be operated near the optimal operating point. At each reference, a lead-lag transfer function and an integrator are used for speed and acceleration control. Combined with exhaust temperature control, the three signals are passed to a low-value selector. The obtained control signal is used to modify the fuel valve position and follow the power output set-point.

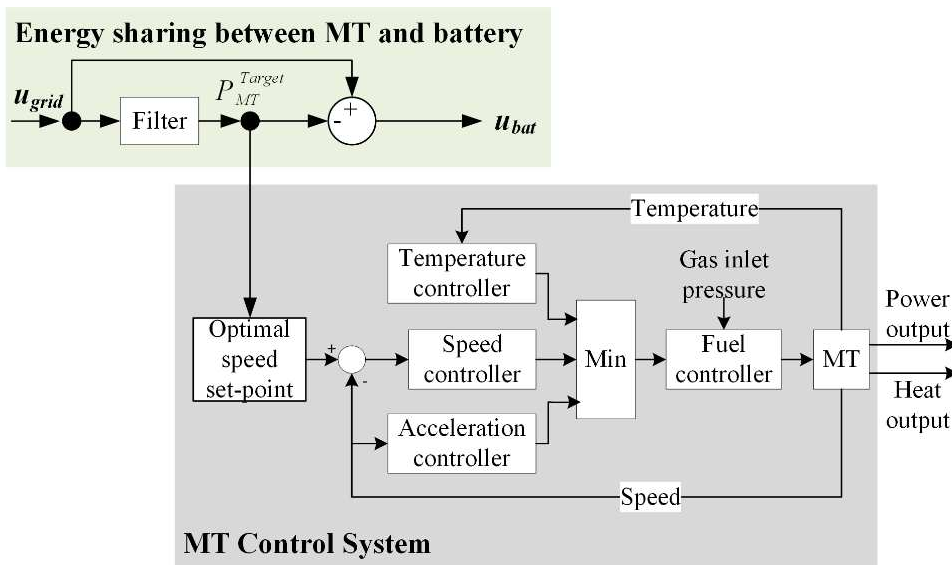


Fig. 3. Energy sharing scheme between the battery and MT.

Referring to the configuration of the existing gas turbine [30], the minimum activation value among temperature, speed, and acceleration controllers is chosen to control the fuel injection. This setup is used to ensure the security of the gas turbine. For example, the output from the acceleration controller may be a big value that is much higher than the temperature controller output. This will lead to a sudden increase in fuel input. The burning of this fuel will then go beyond the capability of the cooling system and result in a high temperature of the gas turbine, which will reduce the lifetime of the turbine or even damage the turbine. By choosing the minimum value, the final output of the controller will ensure that the turbine is operated within

all the limits.

If a battery is used to support MT for frequency response is shown in Fig. 4. The battery supports MT ramping for downward regulation by absorbing electricity (charging) and upward regulation by releasing electricity (discharging). The SoC of the battery is restored when the frequency restores to the baseline so that the battery can be used for the next event.

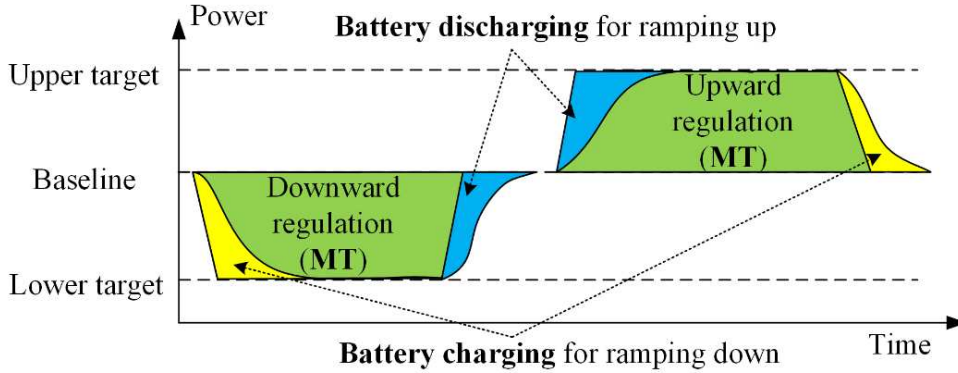


Fig. 4 Principle of using batteries to support MT for regulations.

When the frequency is high or the B-CHP is restoring its power output from a low-frequency event, a downward regulation signal will be sent to the B-CHP. The grid-side inverter decreases its power output according to u_{Grid} . The battery follows the set-point u_{Bat} and absorbs fast change energy from the DC link. Then the MT can change its power output at a slower rate. When the frequency is low or the B-CHP is restoring its power output from a high-frequency event, an upward regulation signal will be sent to the B-CHP. The battery releases energy to avoid fast response of the MT at the DC link.

B. Filter-Based Controller

Fig. 5 presents the details of the filter-based controller in Fig. 3. The battery power output can be scheduled to achieve pre-planned output regulation $\Delta P_{Bat}^{res}(t)$ if required, such as battery state restoration. $\Delta P_{CHP,e}^{target}(t)$ is added on $\Delta P_{Bat}^{res}(t)$ as the target for battery. The battery is used to compensate for the mismatch between $\Delta P_{MT}^{set}(t)$ and $\Delta P_{CHP,e}^{target}(t) + \Delta P_{Bat}^{res}(t)$, so that the total electricity output can be quickly changed to follow the required power output variations. Each set-point is limited by ramping restrictions and capacities. When

the battery SoC is out of limits, the filler will be by-passed. The MT maximizes its response speed to follow frequency response requirements.

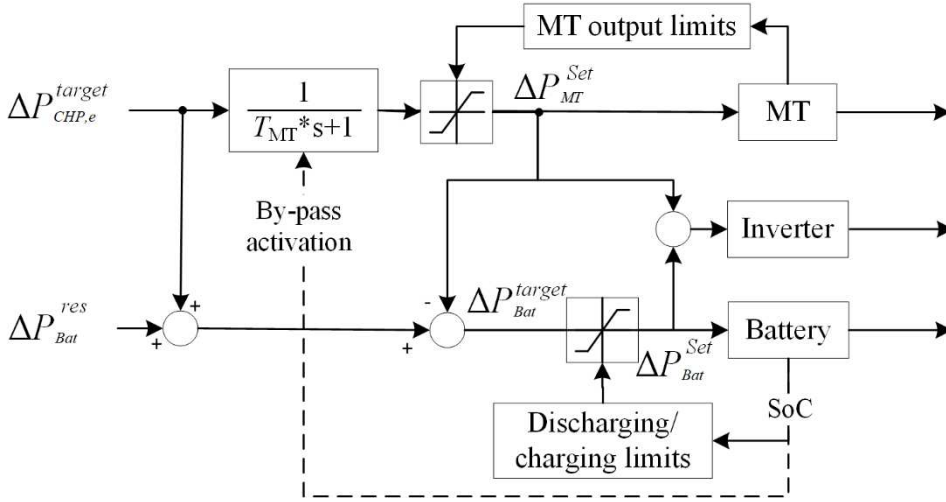


Fig. 5. Flowchart of the filter-based controller.

1) MT Power Output Control

With a given step-change frequency Δf , the flexibility set-point from MT filter output $\Delta P_{MT}^{target}(t)$ is expressed as

$$\Delta P_{MT}^{target}(t) = P[\Delta f] \left(1 - e^{-\frac{t}{T_{MT}}}\right) \leq P_{bid} \left(1 - e^{-\frac{t}{T_{MT}}}\right) \quad (8)$$

According to (C1), the variation of $\Delta P_{MT}^{target}(t)$ satisfies

$$\frac{d}{dt} \Delta P_{MT}^{target}(t) \leq \frac{P_{bid}}{T_{MT}} (1 + \varepsilon) \leq \bar{R}_{MT} \quad (9)$$

$$\left| \frac{d}{dt} \Delta P_{MT}^{target}(t) \right| \leq \frac{P_{bid}}{T_{MT}} (1 + \varepsilon) \leq \underline{R}_{MT} \quad (10)$$

where \bar{R}_{MT} and \underline{R}_{MT} are rates of the MT for ramping up and ramping down, which are not constant when MT power output changes [29]. To ensure system security, these rates are chosen as the minimum values within concerned power output levels.

To ensure that the required flexibility from MT is within the limits for ramping up and ramping down, the minimum allowed time constant of the MT filter T_{MT}^{min} is expressed as

$$T_{MT}^{min} = \frac{P_{bid}}{\min \{ \bar{R}_{MT}, |\underline{R}_{MT}| \}} \quad (11)$$

A larger time constant can further smooth MT output variations without affecting the response accuracy. Yet, a larger time constant will result in a slower response of the MT, and thus more power will be needed from the battery to cover the mismatch between the MT output and the required response. More power from batteries leads to higher capital costs. For frequency deviations smaller than the maximum value, T_{MT}^{min} is large enough for smoothing MT operation unless the owner has other concerns on ramping processes, such as mitigating the impact of gas pressure change on other gas demands or avoiding overheating in the heat supply system.

According to (C2), the amplitude of MT flexibility is limited by the upper limit $\bar{P}_{MT}(t)$ and lower limit $\underline{P}_{MT}(t)$, which are expressed as

$$\bar{P}_{MT}(t) = P_{MT}^{max} - P_{Base}(t) \quad (12)$$

$$\underline{P}_{MT}(t) = P_{MT}^{min} - P_{Base}(t) \quad (13)$$

where $P_{Base}(t)$ is the power output of MT at time t .

The set-point for MT output change $\Delta P_{MT}^{set}(t)$ is expressed as

$$\Delta P_{MT}^{set}(t) = \begin{cases} \bar{P}_{MT}(t), & \Delta P_{MT}^{target}(t) \geq \bar{P}_{MT}(t) \\ \underline{P}_{MT}(t), & \Delta P_{MT}^{target}(t) < \underline{P}_{MT}(t) \\ \Delta P_{MT}^{target}(t), & others \end{cases} \quad (14)$$

For the MT, the available capacity for output change can be sustained if the fuel is available. Upper bound \bar{E}_{MT} and lower bound \underline{E}_{MT} of stored flexibility are thus considered as infinite.

2) Battery Power Output Control

This study considers the support from the battery in two aspects: the ramping process for frequency response and the deficit response caused by the MT capacity limit.

For the ramping support, the target for battery power output $\Delta P_{Bat}^{target}(t)$ is calculated by

$$\Delta P_{Bat}^{target}(t) = \Delta P_{CHP,e}^{target}(t) - \Delta P_{MT}^{set}(t) + \Delta P_{Bat}^{res}(t) \quad (15)$$

The energy stored in the battery $E_{Bat}(t)$ is described by

$$E_{Bat}(t) = \int_{t_0}^{t_0+T_{FR}} [\Delta P_{Bat}^{target}(t) + \Delta P_{Bat}^{res}(t)] \eta_{bat} dt + E_{Base} \quad (16)$$

where η_{bat} represents the charging/discharging efficiency of the battery. For simplicity, it is assumed that the charging and discharging efficiencies are the same. $t \in [t_0, t_0 + T_{FR}]$.

The target for battery power output satisfies

$$P_{Bat}^{min} \leq \Delta P_{Bat}^{target}(t) + \Delta P_{Bat}^{res}(t) \leq P_{Bat}^{max} \quad (17)$$

where P_{Bat}^{min} and P_{Bat}^{max} are limits for charging and discharging.

When $E_{Bat}(t)$ approaches the lower and upper bounds which will be discussed in the next section, P_{Bat}^{min} and P_{Bat}^{max} will be restricted to prevent the battery from overcharging or over-discharging. To avoid sudden loss of battery power output which could lead to the failure in frequency response and DC side voltage fluctuation, a discharging security boundary $E_{Bat}^{min,s}$ and a charging security boundary $E_{Bat}^{max,s}$ are set up. P_{Bat}^{min} and P_{Bat}^{max} are adjusted dynamically as follows

$$P_{Bat}^{max} = \begin{cases} 0, & E_{Bat}(t) \leq \underline{E}_{Bat} \\ \bar{P}_{Bat} \left(\frac{E_{Bat}(t) - \underline{E}_{Bat}}{E_{Bat}^{min,s} - \underline{E}_{Bat}} \right), & \underline{E}_{Bat} < E_{Bat}(t) \leq E_{Bat}^{min,s} \\ \bar{P}_{Bat}, & E_{Bat}^{min,s} < E_{Bat}(t) \end{cases} \quad (18)$$

$$P_{Bat}^{min} = \begin{cases} \underline{P}_{Bat}, & E_{Bat}(t) \leq E_{Bat}^{max,s}(t) \\ \underline{P}_{Bat} \left(\frac{\bar{E}_{Bat} - E_{Bat}(t)}{\bar{E}_{Bat} - E_{Bat}^{max,s}} \right), & E_{Bat}^{max,s} < E_{Bat}(t) \leq \bar{E}_{Bat} \\ 0, & \bar{E}_{Bat} < E_{Bat}(t) \end{cases} \quad (19)$$

where \underline{P}_{Bat} and \bar{P}_{Bat} are maximum charging and discharging power during normal operations. \underline{E}_{Bat} and \bar{E}_{Bat} are the minimum and maximum stored energy in the battery.

The battery power output is designed to enable that the battery can meet the maximum frequency response demand on its own, in case the MT cannot respond within the allowed deadband period. The ramp rate of

battery power output is above the minimum required ramp rate P_{bid}/T_r .

3) Grid-Side Power Output Control

The frequency response demand with all limits is reflected by the obtained set-points for flexibility provision. The obtained set-points of the battery and MT are added up to control the inverter power output, which is expressed as

$$\Delta P_{BCHP}^{set}(t) = \Delta P_{MT}^{set}(t) + \Delta P_{Bat}^{set}(t) \quad (20)$$

The flexibility provided by the B-CHP is described by

$$\mathbf{F}_{BCHP}[\Delta f(t)] = \begin{bmatrix} \frac{d[\Delta P_{MT}^{set}(t)]}{dt} + \frac{d[\Delta P_{Bat}^{set}(t)]}{dt} \\ \Delta P_{BCHP}^{set}(t) \\ \int_{t_0}^{t_0+T_{FR}} \Delta P_{BCHP}^{set}(t) dt \end{bmatrix} \quad (21)$$

IV. SIZING OF THE BATTERY TO SUPPORT THE COORDINATIVE CONTROL

Based on the parameters of the coordinative controller in the last section, a sizing scheme is proposed for designing the power and energy capacities of the battery for supporting the CHP in providing either positive or negative response. Fig. 6 shows the set-point given by the MT filter $\Delta P_{MT}^{set}(t)$ in response to the required frequency response $P_{FR}(t)$.

1) Minimum Rated Power Output

For the duration of frequency response, the required power output of MT $\Delta P_{MT}^{set}(t)$ is expressed as

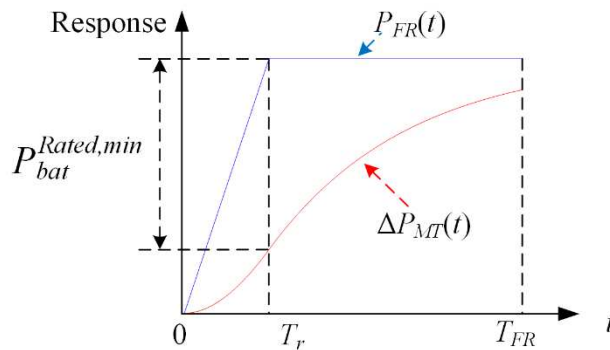


Fig. 6. Power and energy capacity estimation of the battery.

$$P_{MT}(t) = \begin{cases} \frac{k_{FR}\Delta f}{T_r} \left[t - T_{MT} \left(1 - e^{-\frac{t}{T_{MT}}} \right) \right], & 0 \leq t \leq T_r \\ [k_{FR}\Delta f - P_{MT}(T_r)] \left(1 - e^{-\frac{t-T_r}{T_{MT}}} \right) \\ \quad + P_{MT}(T_r), & T_r < t \leq T_{FR} \end{cases} \quad (22)$$

To ensure that the battery can support the CHP during the frequency response period, the minimum required rated power output of the battery $P_{Bat}^{rated,min}$ is chosen as the maximum power output within the frequency response period as follow

$$P_{Bat}^{rated,min} = \max_{\substack{0 \leq t \leq T_{FR}, \\ |\Delta f| \leq \Delta f_{max}}} \{P_{FR}(t) - P_{MT}[\Delta f(t)]\} = \frac{k_{FR}\Delta f_{max}T_{MT}}{T_r} \left(1 - e^{-\frac{T_r}{T_{MT}}} \right) \quad (23)$$

2) Minimum Rated Energy Capacity

During the frequency response period, the required energy capacity of the battery $C_{Bat}[\Delta f]$ is calculated by

$$C_{Bat}[\Delta f] = \int_{t=0}^{T_r} \frac{k_{FR}\Delta f T_{MT}}{T_r} \left(1 - e^{-\frac{t}{T_{MT}}} \right) dt \\ + \int_{t=T_r}^{T_{FR}} \left[\frac{k_{FR}\Delta f T_{MT}}{T_r} \left(1 - e^{-\frac{T_r}{T_{MT}}} \right) e^{-\frac{t-T_r}{T_{MT}}} \right] dt \quad (24)$$

Define the SoC of battery $S_{bat}(t)$ as

$$S_{bat}(t) = \frac{E_{Bat}(t) - \underline{E}_{Bat}}{\bar{E}_{Bat} - \underline{E}_{Bat}} \times 100\% \quad (25)$$

The SoC of battery is limited within a range to maintain the lifetime of the battery. In normal operations, the SoC of the battery is maintained at around 50%. Thus, to ensure that the B-CHP is effective in both high-frequency and low-frequency conditions, the minimum rated energy capacity $C_{Bat}^{rated,min}$ is chosen as twice of the required capacity, which is expressed as

$$C_{Bat}^{rated,min} = \frac{\max_{|\Delta f| \leq \Delta f_{max}} C_{Bat}[\Delta f]}{(\bar{S}_{Bat} - \underline{S}_{Bat})/2} = \frac{2C_{Bat}[\Delta f_{max}]}{\bar{S}_{Bat} - \underline{S}_{Bat}} \quad (26)$$

where \underline{S}_{Bat} is the minimum SoC. \bar{S}_{Bat} is the maximum SoC. $C_{Bat}[\Delta f_{max}]$ is the required energy capacity of the battery to provide frequency response to an event with a maximum frequency deviation at Δf_{max} .

V. CASE STUDIES

In this section, the B-CHP is tested for the FFR in GB electricity market [17]. Fig. 7 presents the B-CHP embedded in a local energy system. The B-CHP absorbs fuel from a gas network and supplies heat and electricity to customers and the power grid. The nominal power output and ramp rate of MT used in the CHP are 30kW and 0.5kW/s, respectively. The gauge pressure of natural gas from the external gas grid at node 1 is 5kPa. The B-CHP and other gas loads are connected to the gas network at node 3 and 4. Details of the gas network and MT can be found in [30][31]. The whole system is implemented in MATLAB/Simulink.

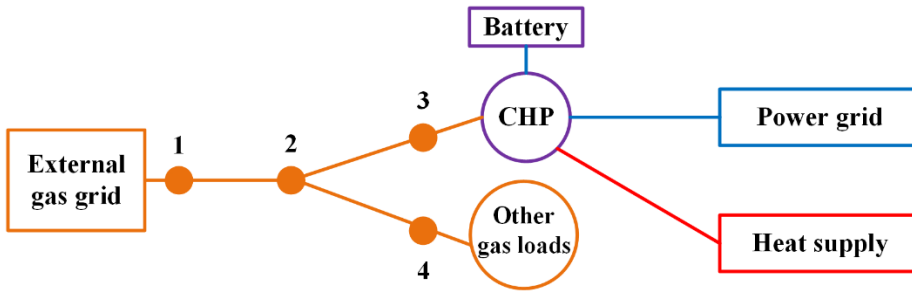


Fig. 7. The layout of the B-CHP for frequency response tests.

A. Grid Frequency Response Test

In this case, an event with a frequency drop is obtained from the GB power grid in 2016 [32]. The frequency response is activated at 65s (see Fig. 8). As an example, the B-CHP provides 8.25kW of its capacity for primary frequency response. According to the proposed battery sizing method, the time constant for the MT T_{MT} is set at 16.5s. The minimum required value of the discharging power of the battery is 6.19kW. For simplicity, the charging power of the battery is chosen at the same value at 6.19kW. Assume that the minimum and maximum SoC are 20% and 80%, respectively, then the minimum required capacity from the battery is 0.118kWh.

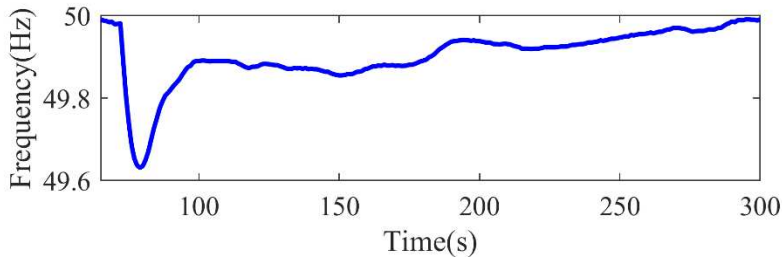


Fig. 8. Variation of grid frequency [32].

Three scenarios are presented to show the effectiveness of the proposed coordinative scheme in releasing the flexibility of CHP. As illustrated in Table I, a CHP without a battery is studied as a reference. The MT is operated at the maximum ramp rate. A battery of 0.118kWh obtained from the previous test is used in three scenarios. In scenario 1, the ramping support from the battery to the CHP is tested for frequency response with the same baseline of CHP generation as that in scenario 0. In scenario 2, a higher baseline generation level of the B-CHP is tested to show additional support from the battery besides ramping. In scenario 3, the battery with low initial SoC is studied to show the potential response failure.

TABLE I

SCENARIOS OF THE BATTERY AND CHP

Scenario	The baseline of CHP generation	Battery installed	Initial SoC of the battery
0 (Reference)	21.0 kW	No	N/A
1	21.0 kW	Yes	53 %
2	27.8 kW	Yes	53 %
3	21.0 kW	Yes	31 %

1) *Scenario 1: Ramping Support from the Battery*

Scenario 1 is carried out to study the ramping performance of the B-CHP for primary frequency response. The baseline of CHP generation is 21.0kW.

Fig. 9 shows the required response and the total generation from the CHP system. Some mismatch is observed between CHP generation of the reference scenario (red line) without a battery and the required

response (blue line) calculated from frequency deviation. In Scenario 1, with the support of the battery, the B-CHP can follow the required response accurately throughout the whole simulation period.

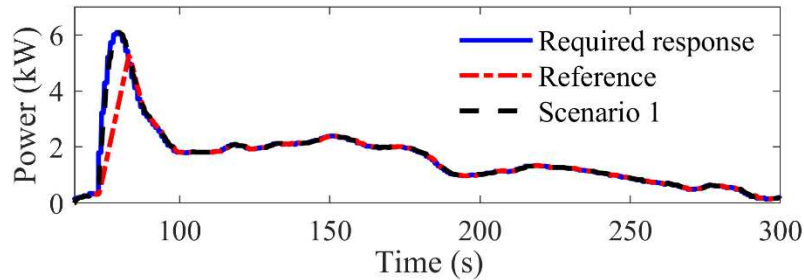


Fig. 9. Frequency response from the B-CHP system.

Fig. 10 shows the generation of CHP during the frequency response. Although CHP without a battery (Reference) has reached its maximum ramp rate, the relevant response is still less than required (see Fig. 9). On the contrary, the CHP with a battery (Scenario 1) can provide an appropriate response with less demand on the CHP ramp rate. The maximum generation of Scenario 1 is around half of the reference scenario. Moreover, it is observed that the CHP generation is well smoothed (see the dashed-black line). With less amplitude of CHP generation variations, it can be expected that the impact of frequency response on the gas network is also mitigated.

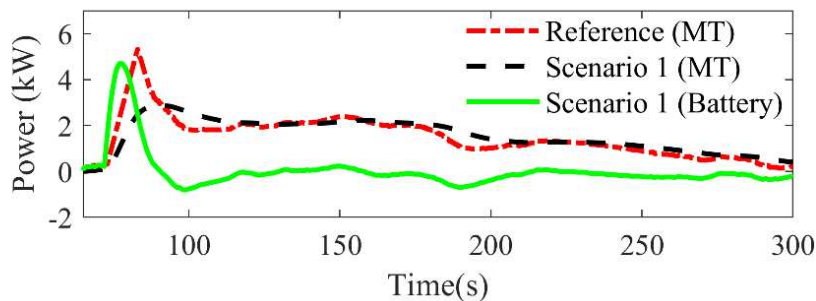


Fig. 10. Power output variations of MT and battery after frequency drop.

Fig. 11 shows the variation of the inlet pressure of the MT. In the reference scenario, a significant pressure drop occurs due to the increasing use of gas for frequency response. In Scenario 1, the maximum pressure drop caused by frequency response decreases to 48.9% level of the reference scenario. Also, small-scale fluctuations of pressure at the inlet of CHP is mitigated.

2) Scenario 2: Amplitude Support from the Battery

Scenario 2 is carried out to study the B-CHP when its baseline is close to the maximum output of CHP.

Scenario 2 is considered with the baseline of CHP generation at 27.8kW.

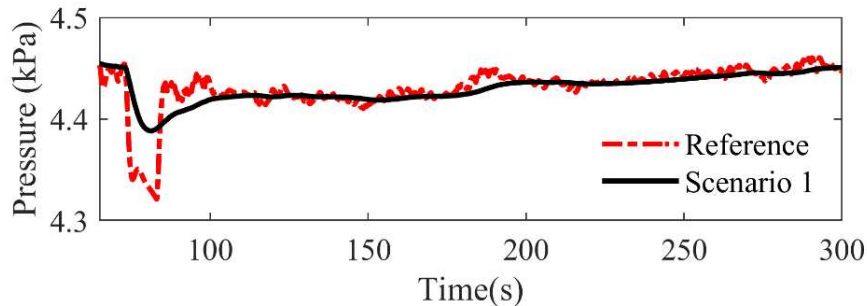


Fig. 11. Inlet pressure of the B-CHP after frequency drop.

Fig. 12 shows that the total electricity output of the B-CHP can follow the demands of frequency response even if the MT is operated at a high level of baseline. It should be noted that the MT cannot fully follow the set-point given by the filter due to the upper generation limits. The mismatch between the set-point and MT output is compensated by the battery discharging.

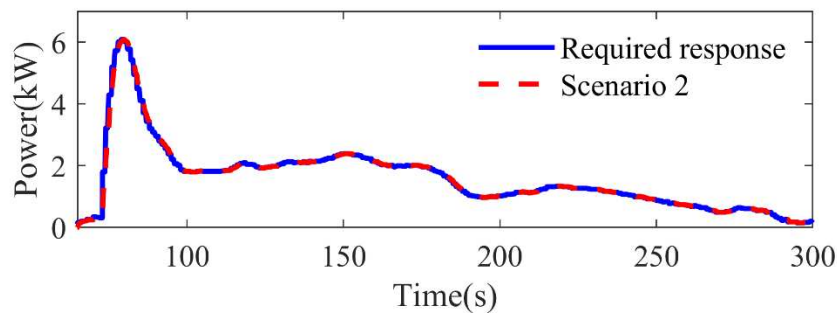


Fig. 12. Frequency response from the B-CHP system.

This support shows that the battery can further enhance the CHP's performance by providing the frequency response on itself when MT power output are partly or fully restricted. However, this support is based on the additional consumption of battery as shown by the dashed green line in Fig. 13. When the required value of power output from the battery is high, the battery will lose the capability for supporting the next event.

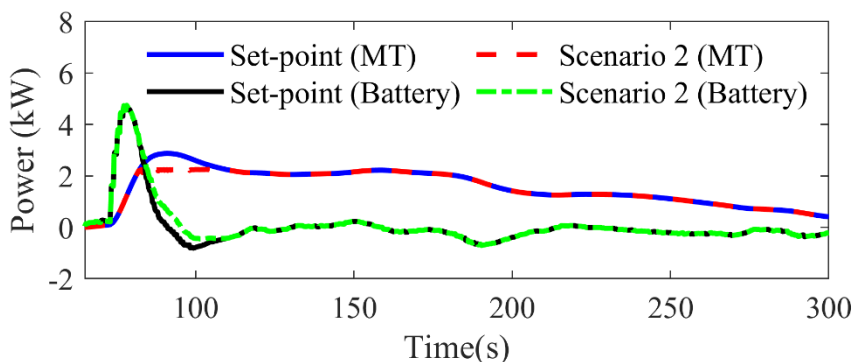


Fig. 13. Power output variations of the MT and battery after frequency drop.

3) Scenario 3: Battery with Low SoC

Scenario 3 is undertaken by studying the performance of CHP with the battery at a low initial SoC (31%). The baseline of CHP generation is assumed to at 21 kW.

As shown in Fig. 14, the SoC goes below 30% at 78.2s. The discharging of the battery is then restricted, so the amplitude of SoC reduction is smaller than other scenarios. The discharging of the battery cannot follow the set-point given by the filter.

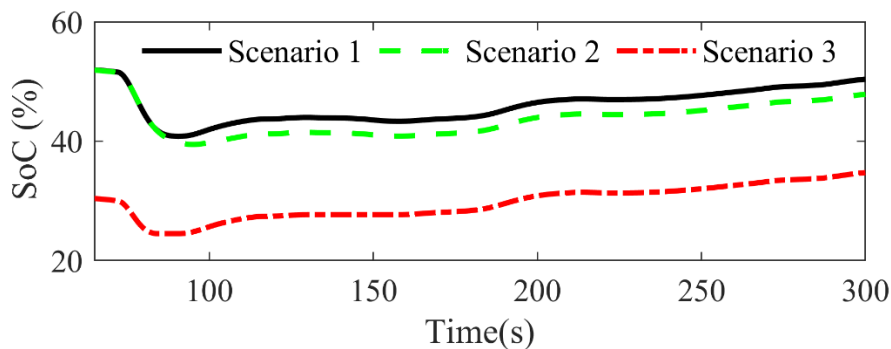


Fig. 14. SoC of the battery.

To follow the frequency response, the MT output set-point by-passes the filter and maximize its response speed as shown in Fig. 15. The results show that the transition period of MT is accomplished smoothly. Although the required frequency response cannot be fully satisfied by the B-CHP system due to the response speed limits (see Fig. 16), the frequency response of B-CHP is still much better than the reference scenario.

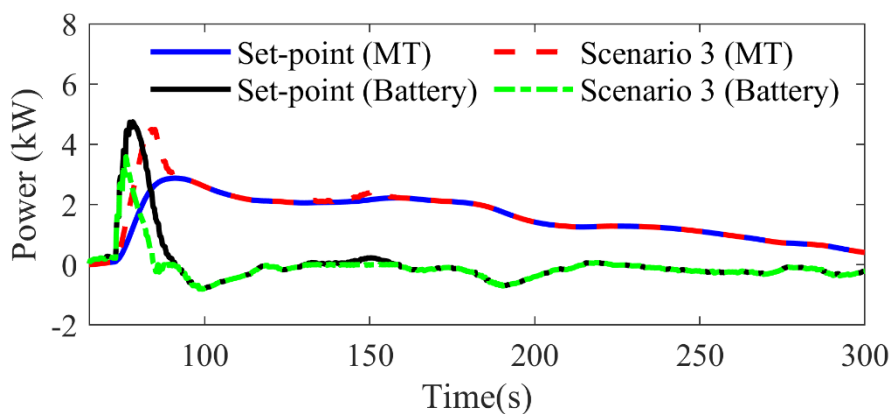


Fig. 15. Power output variations of the MT and battery after frequency drop.

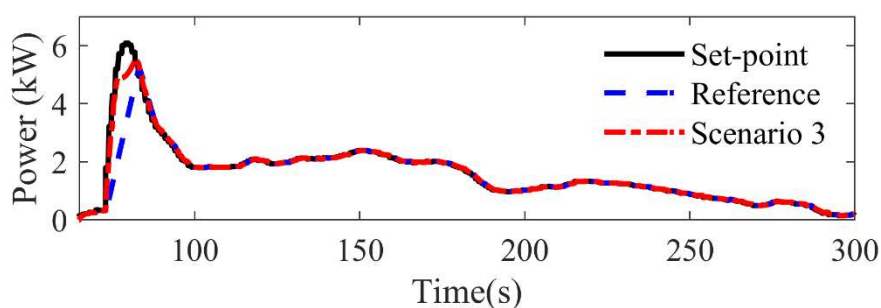


Fig. 16. Frequency response from the B-CHP system.

B. Frequency Response Test in the GB Power System

A simplified GB power system model was used to test the performance of frequency response from B-CHPs. The power system model was extracted from a low-frequency incident that occurred on 27 May 2008 and validated by a detailed model in [33]. The incident caused by a loss of two generators (345MW and 1237MW) within two minutes (the total demand was 41 GW). An inertia constant (H) of 6.5s was used to approximate the response of the power system during the frequency incident. Two lumped generators (G1, G2) were used to model the GB generation system. G1 provides only primary response while G2 provides primary and secondary responses. In Fig. 17, K was chosen as 0.8 which represents 80% of generators provide both responses. Details of the model can be found in [34].

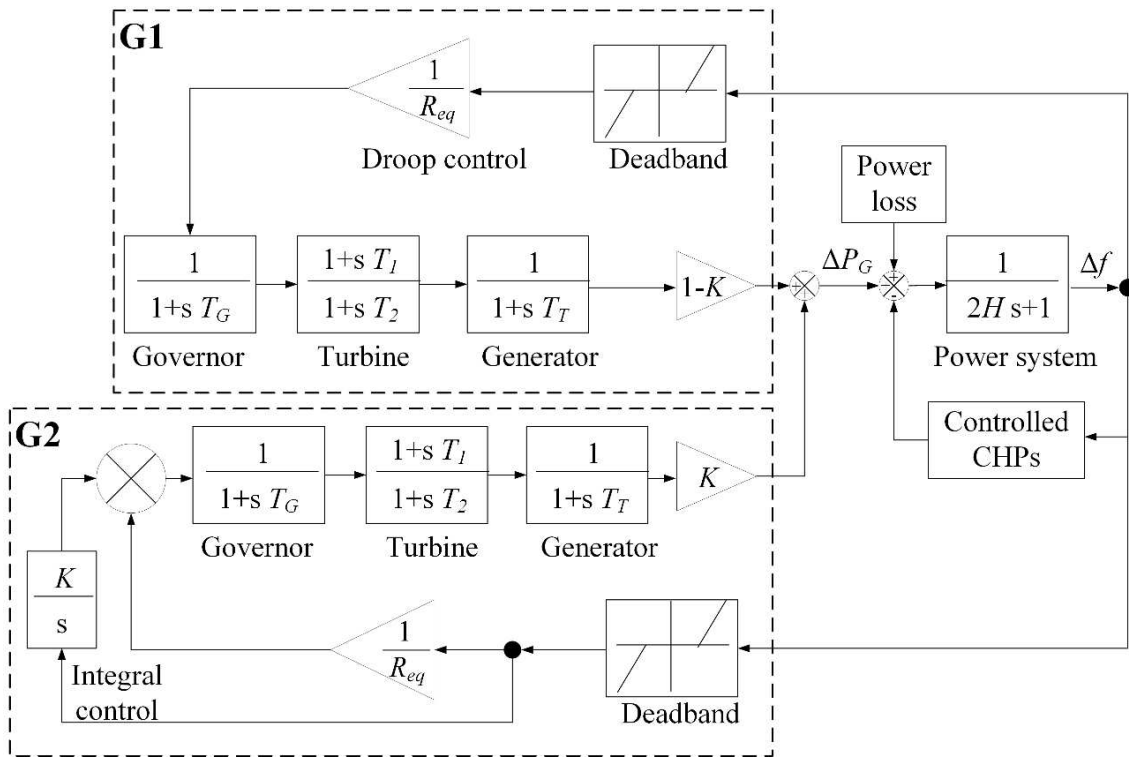


Fig. 17. Simplified GB power system model.

A case study was undertaken considering 30,000 CHPs connected to the power system. Comparisons were carried out between the proposed coordinative controller and the controller in [10] which also updates the control scheme of CHPs to provide frequency response. During the incident, the first loss of generator (345MW) was applied to the GB model at 5s. The second loss of generator (1,237MW) was applied to the GB model at 100s. For simplicity, parameters of the CHP at the start of this section (30kW capacity and 0.5kW/s ramp rate) were used for all the CHPs. Following the setup in scenario 1, each B-CHP provides a maximum response of 8.25 kW to the power grid. 0.118kWh of the battery capacity is used for supporting the CHP. At the start of the incident, the SoC of the battery is 50% while the CHP power output is 21kW.

Fig. 18 shows the variation of grid frequency during the incident. With the proposed coordinative controller, the B-CHPs could coordinate CHP generators and batteries to increase the minimum grid frequency from 49.2Hz to around 49.3Hz (see the dotted red line) after the loss of 1,237MW. By contrast, if using controller in [10] to provide this service, the minimum grid frequency was only 42.27 Hz (see the dashed green line).

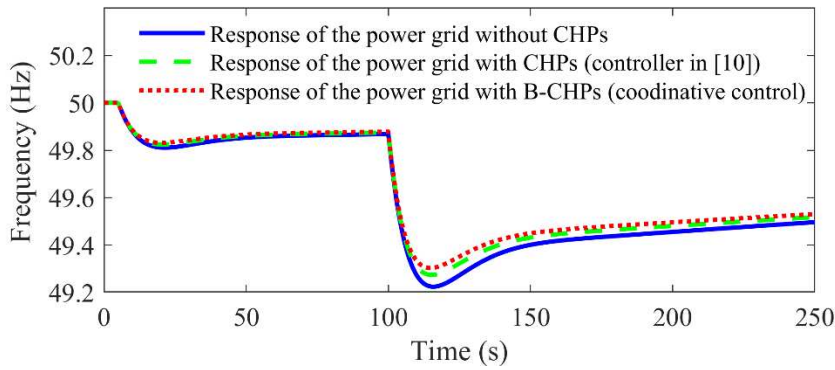


Fig. 18. Variation of grid frequency after the loss of generation.

Meanwhile, as shown in Fig. 19 when the coordinative controller was used, the ramp requirement from CHP generators (see the dotted red line) is mitigated compared with the ramping process of the CHP with the controller in [10] (see the dashed green line). After the incident, the power output of CHP generators remains at a high level and produces excess energy for charging the battery (see the purple line below zero). This feature benefits the state restoration of batteries for the next support to CHPs.

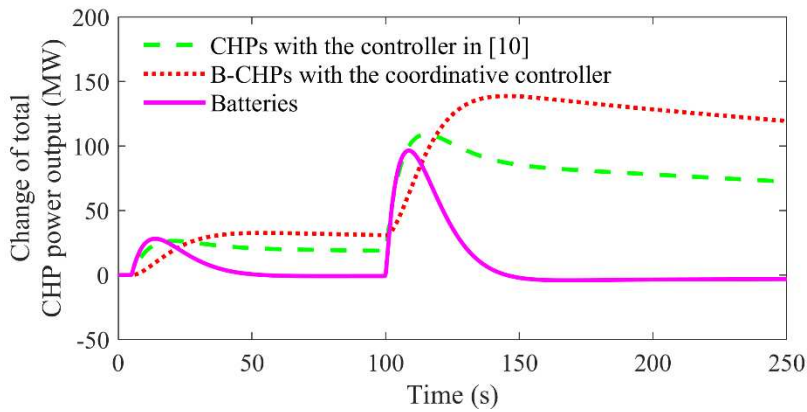


Fig. 19. Change of total power output from CHPs and batteries.

The results show that the proposed controller has better performance in reducing the frequency drop of the power grid while mitigating the reliance on CHP ramping. Although these benefits rely on the function of the battery, the cost-effectiveness analysis in Section V-C has shown that it is economic viable for this instalment. An interval between two services may be required for restoring battery states when two high-frequency or low-frequency events occurred within a short period.

C. Cost-Benefit Analysis

Providing frequency response brings profits to facility owners, which varies under different market conditions. In the dynamic FFR scheme in GB, frequency response is further divided into three subcategories, i.e. primary response, secondary response, and high-frequency response. Primary and secondary responses are called when the frequency deviation moves below -0.015Hz . Primary response is required to be provided within 10s and to be sustained for a further 20s, while secondary response is required to be provided within 30s and to be sustained for a further 30min. High-frequency response is called when the frequency deviation moves over $+0.015\text{Hz}$, and is required to be provided within 10s. Regarding remuneration, the unit prices of availability for providing primary and secondary responses are $\text{£}8.78/\text{MW}/\text{h}$, while the unit price of availability for providing high-frequency response is $\text{£}4.39/\text{MW}/\text{h}$ [35]. For simplicity, it is assumed that the B-CHPs provide the same amplitude (8.25kW , as described in Section V-A) of primary, secondary and high-frequency responses.

In Section V-A, a battery with a maximum discharging power of 6.19 kW is used to avoid the CHP operated at its maximum ramp rate $0.5\text{kW}/\text{s}$. The maximum response that can be provided by a CHP without battery is 5kW for primary and high-frequency responses ($0.5\text{kW}/\text{s} \times 10\text{s}$). The battery smooths the power output of the CHP while enables it to provide an extra 3.25kW for both primary and high-frequency responses (indicating an extra 97.5MW in total for the 30,000 B-CHPs discussed in Section V-B). To enable the B-CHP to provide the same amount (3.25 kW) of extra secondary response, a battery with an energy capacity larger than 0.118kWh (given in Section V-A for primary response) is needed, as the responses are required to be sustained for 30min. Considering the SoC limits (between 20% and 80%) and the requirements for charging and discharging, the battery capacity for each B-CHP is chosen to be 5.4kWh , i.e. $3.25\text{kW} \times 0.5\text{h} \times 2 / (80\% - 20\%)$ referring to (26).

The benefit of providing extra amounts of frequency response services (97.5MW) due to the battery installation equals to $\text{£}12,498,330/\text{year}$, according to (27). Referring to [36], the battery price is considered as $\text{£}121/\text{kWh}$, with which, the total cost of installing 5.4kWh batteries with converters in 30,000 B-CHPs can

be estimated by (28). However, the converter cost changes at various configurations and market conditions. Fig. 20 compares the static payback periods of installing batteries at various ratios of the converter cost to the battery cost. The results range from 1.57 to 3.14 years. Furthermore, as the battery is usually not fully used when providing frequency response services, the payback period can be further reduced if the battery is also used to make profits from other services such as peak shaving. Besides, some CHPs already have batteries installed for other purposes, such as load shifting and engine start-up in the standalone mode [28]. These batteries may also be used for providing frequency response at the same time, so that there can be little or less need to install extra batteries. In this case, the cost-effectiveness of batteries can be justified more easily.

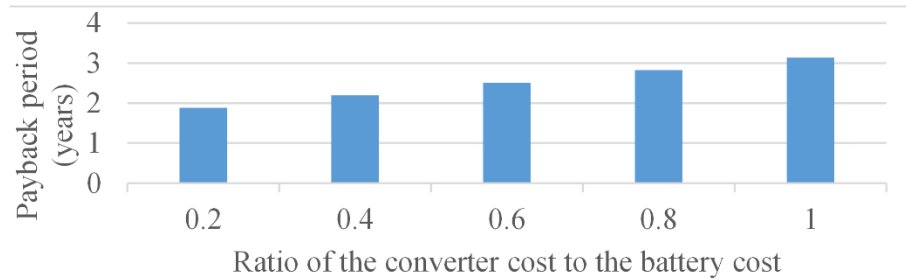


Fig. 20. Variation of static payback period under various converter costs.

VI. CONCLUSION

In this paper, a filter-based coordinative control scheme is proposed to unlock the flexibility of a CHP for frequency response by using batteries. The time constant of the filter which is conventionally determined through the trial and error method is designed considering the ramp restrictions of the original CHP. The required capacities of battery for compensating the mismatched power between CHP generation and required response is identified based on the time constant.

Numerical results show that a battery can enhance the capability of a CHP for frequency response, and the cost of the required battery is minor compared with the high cost of the CHP. In practice, the capacity of batteries should have some conservativeness to ensure system security. It is also found that the battery can not only increase the ramp rate of the CHP, but also balance the excess/deficit capacity when the CHP is

operated near the maximum or the minimum outputs. With the proposed scheme, the battery mitigates the adverse impact of frequent generation regulation on the lifetime of the turbine and the pressure level of the gas network. The control scheme and the sizing method can be applied to a CHP with a larger capacity based on the demand for flexibility.

This paper focuses on the coordinative control of CHP and electricity storage in providing frequency response services. The battery is used as an example of electricity storage since some CHPs already have onboard batteries. If not equipped with batteries, other solutions such as supercapacitors or flywheels which respond faster than batteries [37], are also suitable for this kind of support operations. In fact, supercapacitors could be even cheaper than batteries for short-term power support. Moreover, it is easier to install these solutions in the DC link of the machine. In future work, more comprehensive comparisons will be conducted to consider CHP's requirements on energy and power storage systems for different applications.

APPENDIX

The profit from providing FFR services to the power grid EP_{FFR} can be expressed as

$$EP_{FFR} = (c_p \times P_p + c_s \times P_s + c_h \times P_h) \times D_{fr} \times N_{yr} \quad (27)$$

where c_p , c_s , and c_h represent the unit prices of availability for providing primary, secondary, and high-frequency responses, respectively. P_p , P_s , and P_h represent the tendered amplitudes for providing primary, secondary, and high-frequency responses, respectively. N_{yr} is the number of days per year. D_{fr} is the windows size for providing the responses. This paper uses 16h/day as D_{fr} . This number is chosen from historical tenders in a real GB dataset [38], where D_{fr} ranges from 4h to 24h.

The cost of battery installment CAP_{bat} includes the battery cost and the DC/DC converter cost, which is expressed as

$$CAP_{bat} = c_{bat} \times E_{bu} \times (1 + \alpha) \times N_{bat} \quad (28)$$

where c_{bat} is the battery price per kWh. E_{bu} is the size of a battery unit. N_{bat} is the number of battery units. α is the ratio of the converter cost to the battery cost.

REFERENCES

- [1] Q. Wang, and B. M. Hodge. "Enhancing power system operational flexibility with flexible ramping products: A review," *IEEE Trans. Ind. Informat.*, vol. 13, no. 4, pp. 1652-1664, Dec. 2016.
- [2] "Status of power system transformation 2018." International Energy Agency, 2018. [Online]. Available: <https://webstore.iea.org/download/summary/1041>. Access on: Mar. 09, 2019.
- [3] "Electricity system flexibility." The Office of Gas and Electricity Markets (Ofgem), 2018. [Online]. Available: <https://www.ofgem.gov.uk/electricity/retail-market/market-review-and-reform/smarter-markets-programme/electricity-system-flexibility>). Access on: Dec. 29, 2018.
- [4] H. R. Chamorro, et al., "Innovative primary frequency control in low-inertia power systems based on wide-area RoCoF sharing," *IET Energy Systems Integration*, vol. 2, no. 2, pp. 151–160, Feb. 2020.
- [5] "Electricity Generation Costs and Hurdle Rates." UK Department of Energy and Climate Change, 2016. [Online]. Available: https://assets.publishing.service.gov.uk/government/uploads/system/uploads/attachment_data/file/566803/Leigh_Fisher_Non-renewable_Generation_Cost.pdf. Access on: Feb. 11, 2020.
- [6] "Flexible combined heat and power (CHP) systems." U. S. Department of Energy, 2018. [Online]. Available: https://www.energy.gov/sites/prod/files/2018/01/f47/Flexible%20CHP%20Comms_01.18.18_compliant.pdf. Access on: Feb. 21, 2019.
- [7] G. Wen, et al., "Frequency regulation of source-grid-load systems: a compound control strategy," *IEEE Trans. Ind. Informat.*, vol. 12, no. 1, pp. 69-78, Feb. 2016.
- [8] Y. Zhou, M. Cheng, and J. Wu, "Enhanced frequency response from industrial heating loads for electric power systems," *IEEE Trans. Ind. Informat.*, vol.15, no. 6, pp. 3388-3399, Nov. 2018.
- [9] D. Jones, M. Kelly, "Supporting Grid Modernization with Flexible CHP Systems," ICF [Online], Nov 2017. Available: <https://www.icf.com/resources/white-papers/2017/supporting-grid-modernization-with-flexible-chp-systems>

- [10] Y. Bian, et al., "Frequency response in the GB power system from responsive CHPs," *Energy Procedia*, vol. 105, pp. 2302-2309, 2017.
- [11] N. Liu, et al., "Multiparty energy management for grid-connected microgrids with heat-and electricity-coupled demand response," *IEEE Trans. Ind. Informat.*, vol. 14, no. 5, pp. 1887-1897, Sep. 2017
- [12] J. Riveros, et al., "A new approach for near real-time micro-CHP management in the context of power system imbalances-A case study," *Energ. Conv. & Mana.*, vol. 89, pp. 270-280, Jan. 2015.
- [13] H. Ameli, M. Qadrdan, and G. Strbac, "Coordinated operation strategies for natural gas and power systems in presence of gas-related flexibilities," *IET Energy Systems Integration*, vol. 1, no. 1, pp. 3–13, Jan. 2019.
- [14] X. Xu, W. Sun, M. Abeysekera, and M. Qadrdan, "Quantifying the flexibility from industrial steam systems for supporting the power grid," *IEEE Trans. Power Syst.*, early-access, doi: 10.1109/TPWRS.2020.3007720.
- [15] T. Korpela, et al., "Utilization of district heating networks to provide flexibility in CHP production," *Energy Procedia*, vol. 116, pp:310-319, Jun. 2017.
- [16] "Reciprocating engines: Giving wind farm reliability a lift," *Power Engineering International*, 2007. [Online]. Available: <https://www.powerengineeringint.com/articles/print/volume-15/issue-7/features/reciprocating-engines-giving-wind-farm-reliability-a-lift.html>. Access on: Feb. 17, 2019.
- [17] "Testing guidance for providers of firm frequency response balancing service." National Grid, 2017. [Online]. Available: <https://www.nationalgrid.com/sites/default/files/documents/FFR%20Testing%20Guidance%20verD11%20Final.pdf>. Access on: Feb. 06, 2019.

- [18] “Historic frequency data.” National Grid, 2020. [Online]. Available: <https://www.nationalgrideso.com/balancing-services/frequency-response-services/historic-frequency-data>. Access on: Feb 20, 2020.
- [19] “PJM manual 12: Balancing operations.” PJM, 2019. [Online]. Available: <https://learn.pjm.com/three-priorities/buying-and-selling-energy/ancillary-services-market/regulation-market.aspx>. Access on: Feb. 10, 2020.
- [20] Y. Assoul, et al., “Life estimation of first stage high pressure gas turbine blades,” *Sci. Tech. Rev.*, vol. 58, no. 2, pp. 8-13, Apr. 2008.
- [21] T. G. Isaiah, et al., “Life cycle evaluation of an intercooled gas turbine plant used in conjunction with renewable energy,” *Propul. & Power Research*, vol. 5, no. 3, pp. 184-93, Sep 2016.
- [22] M. Chertkov, S. Backhaus, and V. Lebedev, “Cascading of fluctuations in interdependent energy infrastructures: Gas-grid coupling,” *Appl. Energ.*, vol. 160, pp. 541-551, Dec. 2015.
- [23] Y. Zhou, et al., “An equivalent model of gas networks for dynamic analysis of gas-electricity systems,” *IEEE Trans Power Syst.*, vol. 32, no. 6, pp.4255-64, Nov. 2017.
- [24] “Maximising CHP with demand side response”. Centrica Business Solutions, 2018. [Online]. Available: https://www.centricabusinesssolutions.com/sites/g/files/qehiga126/files/UKUniversity_casestudy.pdf. Access on: Nov 01, 2018.
- [25] Z. Li, et al., “Combined heat and power dispatch considering pipeline energy storage of district heating network,” *IEEE Trans Sustain. Energ.*, vol. 7, no. 1, pp. 12-22, Jan. 2016.
- [26] X. Chen, et al., “A domestic CHP system with hybrid electrical energy storage,” *Energ. & Buildings*, vol. 55, pp.361-368, Dec. 2012.
- [27] “Enhanced Frequency Control Capability (EFCC) --- Battery Storage Investigation Report,” National Grid, 2015. [Online]. Available: <https://www.nationalgrideso.com/document/96486/download>. Access on: Feb. 08, 2020.

- [28] “Capstone microturbine user's manual,” Capstone Turbine Corporation, 2002. [Online]. Available: [https://www.wmrc.edu/projects/BARenergy/manuals/c-30-manuals/400001_C30_C60_MicroTurbine_Users_Manual .pdf](https://www.wmrc.edu/projects/BARenergy/manuals/c-30-manuals/400001_C30_C60_MicroTurbine_Users_Manual.pdf). Access on: Nov. 08, 2018.
- [29] “Behavior of Capstone and Honeywell microturbine generators during load changes.” California Energy Commission, 2001. [Online]. Available: [https://eetd.lbl.gov/sites/all/files/publications/capstone-honeywell-micro turbine-report.pdf](https://eetd.lbl.gov/sites/all/files/publications/capstone-honeywell-micro-turbine-report.pdf). Access on: Feb. 03, 2019.
- [30] D. N. Gaonkar, “Performance of microturbine generation system in grid connected and islanding modes of operation,” Distributed Generation InTech, 2010. [Online]. Available: <https://www.intechopen.com/books/distributed-generation/performance-of-microturbine-generation-system-in-grid-connected-and-islanding-modes-of-operation>. Access on: Feb. 06, 2019.
- [31] X. Xu, et al., “Dynamic modeling and interaction of hybrid natural gas and electricity supply system in microgrid,” *IEEE Trans. Power Syst.*, vol. 30, no. 3, pp. 1212-1221, May. 2015.
- [32] “Historic frequency data,” National Grid Electricity System Operator, 2016. [Online]. Available: <https://www.nationalgrideso.com/balancing-services/frequency-response-services/historic-frequency-data>. Access on: Nov. 12, 2018.
- [33] T. Bopp, “Technical and commercial integration of distributed and renewable energy sources into existing electricity networks,” Ph.D. dissertation, Dept. Electr. Electron. Eng., Univ. of Manchester, Manchester, U.K., 2006.
- [34] M. Cheng et al., “Power system frequency response from the control of bitumen tanks,” *IEEE Trans. Power Syst.*, vol. 31, no. 3, pp. 1769–1778, May. 2016.
- [35] M. Cheng, S. Sami, and J. Wu, “Benefits of using virtual energy storage system for power system frequency response,” *Applied Energy*, vol. 194, pp. 376-385, May. 2017.

- [36] “Battery pack prices fall as market ramps up with market average at \$156/kwh in 2019,” BloombergNEF, 2019. [Online]. Available: <https://about.bnef.com/blog/battery-pack-prices-fall-as-market-ramps-up-with-market-average-at-156-kwh-in-2019/>. Access on: Jan. 12, 2020.
- [37] “Energy storage technology and cost characterization report,” the US Department of Energy, 2019. [Online]. Available: https://www.energy.gov/sites/prod/files/2019/07/f65/Storage%20Cost%20and%20Performance%20Characterization%20Report_Final.pdf. Access on: Feb. 08, 2020.
- [38] “FFR market information and tender reports” National Grid, 2020. [Online]. Available: <https://www.nationalgrideso.com/balancing-services/frequency-response-services/firm-frequency-response-ffr?market-information>. Access on: Jan. 12, 2020.



Xiandong Xu (M’15) received the B.Eng. and Ph.D. degrees in Electrical Engineering from Tianjin University, China, in 2009 and 2015, respectively.

He has been a Research Associate at Cardiff University, UK, since 2017 and an Associate Professor at Tianjin University, China, since 2020. His research focuses on modelling and optimization of integrated energy systems, and flexibility of heat and industrial sectors.



Wenlong Ming (M’16) received the B.Eng. and M.Eng. Degrees in Automation from Shandong University, Jinan, China, in 2007 and 2010, respectively. He received the Ph.D. degree in Automatic Control and Systems Engineering from the University of Sheffield, Sheffield, U.K., in 2015. He was the winner of the prestigious IET Control & Automation

Doctoral Dissertation Prize in 2017.

He has been a Lecturer of Power Electronics at Cardiff University, U.K., since August 2016 and a Senior Research Fellow funded by Compound Semiconductor Applications (CSA) Catapult, U.K., for 5 years since

April 2020. His research interests focus on Medium Voltage DC systems for electricity distribution networks and characterization, modelling, applications of wide-bandgap compound semiconductors.



Yue Zhou (M'13) received the B.S., M.S., and Ph.D. degrees in electrical engineering from Tianjin University, Tianjin, China, in 2011, 2016, and 2016, respectively. He was a postdoctoral research associate in the School of Engineering, Cardiff University, Cardiff, U.K. from 2017 to 2020.

He is currently a Lecturer in Cyber Physical Systems in the School of Engineering, Cardiff University, Cardiff, U.K. His research interests include peer-to-peer energy trading, demand side response and blockchain technology.



Jianzhong Wu (M'04) received his B.S., M.S. and Ph.D. degrees in electrical engineering from Tianjin University, China, in 1999, 2002 and 2004, respectively.

He is currently a Professor of Multi-Vector Energy Systems and Head of School of Engineering at Cardiff University, UK. His research interests include energy infrastructure and smart grid. Prof. Wu is an Associate Editor of Applied Energy. He is a co-Director of UK Energy Research Centre and EPSRC Supergen Hub on Energy Networks.